Tellus (2001), 53A, 129–145
Printed in UK. All rights reserved

TELLUS
ISSN 0280–6495

Ideal shocks in 2-layer flow

Part I: Under a rigid lid

By QINGFANG JIANG and RONALD B. SMITH*, *Department of Geology and Geophysics, Yale University, New Haven, Connecticut 06520-8109, USA*

(Manuscript received 17 May 1999; in final form 2 October 2000)

ABSTRACT

Previous work on the classical problem of shocks in a 2-layer density-stratified fluid used either a parameterized momentum exchange or an assumed Bernoulli loss. We propose a new theory based on a set of viscous model equations. We define an idealized shock in two-layer density stratified flow under a rigid lid as a jump or drop of the interface in which (1) the force balance remains nearly hydrostatic in the shock, (2) there is no exchange of momentum between the two layers except by pressure forces on the sloping interface, and (3) dissipative processes can be treated with a constant viscosity. We proceed in two steps. First, we derive a necessary condition for shock existence based on a requirement for wave steepening. Second, we formulate and solve a set of viscous model equations. Some results are the following: Shocks require strong layer asymmetry; one layer must be much faster and/or shallower than the other layer. The linearized equations describing the shock tails provide boundary conditions and a proof of shock uniqueness. It is possible to derive an analytical solution for weak shocks if the steepening condition is met. The weak shock solutions provide closed form expressions for the Bernoulli loss in each layer. Bernoulli losses are strongly concentrated in the expanding layer as the relative layer depth change is much larger in that layer. Bernoulli losses are independent of layer viscosity. A sudden cessation of shock existence is found for strong shocks when the possible end state migrates into the supercritical regime. Surprisingly, the new ideal shock theory compares well with a 2-D, time-dependent shallow water model (SWM) with a flux formulation, but with no viscous formulation. Both the Bernoulli drop and shock cessation condition agree quantitatively.

1. Introduction

1.1. Review of previous work

Shock theory (i.e., the theory of hydraulic jumps, drops, and bores) in stratified flow has a wide variety of applications in engineering and stratified atmospheric or oceanic flow. While the shock in single layer flow is well understood, the internal shock in two active layers has puzzled scientists for more than half a century.

For a hydraulic jump in a single layer flow, the precise end state and the corresponding dissipation are prescribed by bulk mass and momentum conservation; independent of the details in the jump. In a two layer shock however, there are two additional processes involved: interfacial mixing and momentum exchange due to the pressure on the sloping interface. Although mass conservation in each layer may still be valid, these two unknown momentum exchange processes prevent the direct application of momentum conservation to each individual layer. Some extra assumption is required.

A bulk parameterization of interfacial momentum exchange was proposed by Yih and Guha

* Corresponding author.
e-mail: ronald.smith@yale.edu

(1955, hereafter YG55). They simplified the momentum exchange expression using a mean hydrostatic pressure. The effect of interfacial mixing was ignored. With YG's formulation, the nature of a two layer shock is governed by a pair of coupled quadratic (for rigid lid flow) or cubic (for free surface flow) algebraic equations. YG55 compared their solutions against experiments using two layer fluids with a single active layer. A satisfactory agreement was found for both hydraulic jumps and drops with differing density ratios. The four physical roots from YG55 were further examined by Mehrotra (1973) and Mehrotra and Kelly (1973). Although still widely used, the YG theory has been criticized for its prediction of energy gain in any contracting layer and its suspicious multiple conjugate states across an internal shock (Armi, 1986 and Baines, 1995).

Another set of assumptions was proposed by Chu and Baddour (1974) and Wood and Simpson (1984, hereafter WS84). They assumed that the interfacial mixing is negligible and that energy in the contracting layer is conserved. Hereafter, we refer to this theory as CBWS. During 1980s, experiments on lee jumps and upstream bores of weak or intermediate strength (WS84; Baines, 1984; and Rottman and Simpson, 1989) found reasonable agreement with YG55 and CBWS. However, both theories broke down for strong internal bores, in which turbulent mixing is vigorous.

For weak shocks, Armi (1986) suggested that dissipation in both layers might be negligible. Unlike the YG55 or CBWS formulations, Armi's formulation has a unique conjugate state for a specified upstream state.

Noticing that neither YG's nor CBWS's formulation can well describe strong laboratory generated bores, Klemp, Rotunno, and Skamarock (1997, hereafter KRS97) proposed that energy in the expanding layer should be conserved. KRS97 compared their predictions against both previous experimental data and a set of numerical simulations. Satisfactory agreement was found for internal bores over a wide variety of strengths. An interesting feature of this formulation is that in the gravity current limit, while both YG55 and CBWS break down, KRS97 reduces to the classical gravity current theory (Benjamin, 1968). However, in contrast to its convincing behavior for internal bores, the KRS97 formulation seems inappropriate to describe internal lee jumps (KRS97).

1.2. Assumptions and motivations of ideal shock theory

The goal of this study is to reformulate the two-layer shock problem with simple viscous model equations. We hope that the properties of these equations will teach us something about shocks, without having to make ad hoc assumptions concerning the pressure force on the sloping interface or the Bernoulli loss across the shock. Both of these quantities should be predicted by the theory, instead of being assumed in the beginning. We still require assumptions however. Our assumptions are summarized by the term "ideal shock": (1) interfacial mixing is negligible; (2) the flow is hydrostatic in shocks; and (3) the small scale turbulence can be parameterized by a constant Newtonian or non-Newtonian viscosity.

It is already quite clear, from the illuminating numerical work of KRS97 and the laboratory experiments of WS84, Baines (1984), and Rottman and Simpson (1989), that one type of shock, the strong hydraulic bore, exhibits significant amounts of momentum exchange between layers due to interfacial mixing. In this case, with a large upstream depth ratio, weak upstream shear and a sharp interface, shear generated turbulence and momentum exchange within the shock is considerable and added momentum can significantly modify the Bernoulli value of the thin lower layer and modify the speed of the bore. For most other types of two-layer shocks, including lee shocks and shock flows with thicker interfaces (such as atmospheric or ocean flow) or two-layer flows with comparable depth, momentum exchange either is not dominant or has not yet been shown to be dominant. Thus, the ideal shock assumption may have broad direct application or, at the very least, may provide a framework for further investigation of non-ideal effects.

The hydrostatic assumption, applied in the shock, is another critical aspect of the ideal shock theory. In part I, we consider Newtonian and non-Newtonian representations of these smaller scale processes. Except for internal bores near the gravity current limit, the observed shock width is often twice or thrice the layer depths (e.g., Rouse et al., 1959 and Rottman and Simpson, 1989) suggesting that the hydrostatic approximation might be the appropriate first approximation for the time or ensemble mean flow. However, for undular bores, the wave-like undulations in the shock may violate this assumption. Previous experiments suggested that the undular structure in bores decayed rapidly downstream, and only the first several waves were visible (Baines, 1995). Therefore, we define our shock width to include all the undular waves, and use a smoothed monotonic interface as an approximation of the actual undular interface. These definitions have two physical implications. First, the energy in the undular waves will eventually cascade to turbulence and heat. Therefore, for our definition of the hydraulic jump, no energy propagates out of the jump. Second, the smoothed interface satisfies the hydrostatic assumption. However, there is no doubt that the the non-hydrostatic component ignored by our assumptions may play some role in the interfacial momentum exchange, which further modifies the energy distribution and the end-states of jumps.

The concept of the ideal shock contributes to three aspects of hydraulic jump research. First, it provides a formulation of a class of dissipative non-linear wave equations that can be studied using the methods of applied mathematics and numerical simulation in the same way that the KdV or viscous KdV equation have been analyzed (Whitham, 1974; Baines, 1995). These analyses, while not always directly applicable to real flows, reveal fundamental constraints and balances.

Ideal shock theory also contributes to the understanding of numerical Shallow Water Models (SWM) of non-linear layered flow with jumps. Such models have recently been used to illustrated the generation of potential vorticity in breaking mountain waves (e.g., Schär and Smith, 1993, hereafter SS93; Smith and Smith, 1995, hereafter SS95; and Grubišić et al., 1995) and their qualitative predictions have been successfully compared against atmospheric observations of mountain induced wakes and jets (Grubišić and Smith, 1993; Grubišić et al., 1995; Smith et al., 1997; and Pan and Smith, 1999). The mass/momentum flux-conservative formulation of these models is consistent with the assumptions of ideal shock theory. Thus, ideal shock theory provides a framework for diagnosing these models. Ideal shock theory is also consistent with the pioneering 1-D numerical work of Houghton and Isaacson (1968) and provides further insight into their results.

Finally, ideal shock theory allows the derivation of shock relations which can be tested against existing and future laboratory observations. The failure of such tests would implicate the neglected effects of momentum mixing, turbulence and non-hydrostatic effects.

The outline of this paper is as follows. Finite amplitude steepening theory is developed in Section 2. A viscous internal shock model is constructed in Section 3, similar to the model proposed for a single layer flow by SS95. Analytical solutions are derived for weak shocks in Section 4. Finite shock solutions and viscous tail modes are discussed in Section 5. In Section 6, for comparison with the new theory, high resolution numerical simulations are performed. A summary is given in Section 7.

In a companion paper (Jiang and Smith, 2001), we extend our approach to the case with a passive layer above the basic two-layer system.

2. Finite amplitude wave steepening

As prelude to ideal shock theory, we consider a universal constraint on shock formation; wave steepening. The process of wave steepening to form an infinitesimal shock has been discussed by Long (1954), Mehrotra (1973), and Baines (1984). Here we take a new approach and start with a finite amplitude perturbation.

Assume that we have a steady monotonic perturbation with a finite vertical displacement of the interface η over a finite distance $\widehat{ab}$ (Fig. 1). The perturbation can be either positive ($\eta > 0$) or negative ($\eta < 0$). In a reference frame moving with the perturbation, the flow is steady so that we can define a constant mass flux Q in each individual layer

$$Q_1 = U_1 H = U_1'(H + \eta), \tag{1}$$

$$Q_2 = U_2(D - H) = U_2'(D - H - \eta), \tag{2}$$

where U_1 and U_2 are pre-perturbation flow velocities in the lower and the upper layer relative to the perturbation, H is the lower layer depth, D is the total depth, and U_1' and U_2' are post-perturbation flow velocities in the lower and the upper layer relative to the perturbation.

We propose the following hypothesis: in order

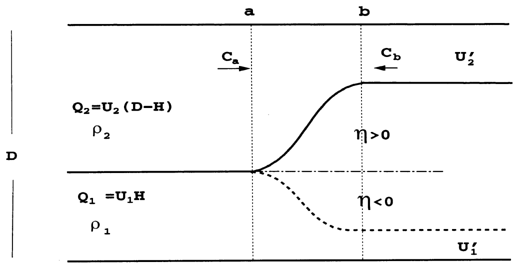

Fig. 1. Definition sketch of a two layer flow system between rigid upper and lower boundaries. A finite monotonic perturbation of the interface η between points "a" and "b" is shown. The perturbation could be positive ($\eta > 0$) or negative ($\eta < 0$, the dashed interface). Density in the lower layer is ρ_1 and in the upper layer is ρ_2, and $\rho_1 > \rho_2$. Q is the volume flux, C is the speed of small waves.

to allow the perturbation to steepen and form a steady shock, it is necessary that the inviscid linear wave speed at the leading edge ("a") must be positive ($C_a > 0$) and the inviscid linear wave speed at trailing edge ("b") must be negative ($C_b < 0$). Here we are only interested in the wave mode propagating against the mean flow. In other words, wave steepening is possible only when the flow at the leading edge is supercritical and a range of possible downstream states can be found which are subcritical. If this condition is met, the leading edge and the trailing edge of the shock can propagate towards each other and allow the perturbation to steepen. A steady shock can exist, if a balance can be reached between the viscous force and the nonlinear inviscid wave steepening tendency.

For a two-layer Boussinesq flow with a rigid lid, the inviscid linear hydrostatic wave speed (the mode propagating against mean flow) can be expressed as (Baines, 1995):

$$C = \frac{Q_1(D-H)}{DH} + \frac{Q_2 H}{D(D-H)} - \sqrt{\frac{H(D-H)}{D^2}\left[g'D - \left(\frac{Q_1}{H} - \frac{Q_2}{D-H}\right)^2\right]}, \quad (3)$$

where $g' = (1-r)g$ is the reduced gravity, and $r = \rho_2/\rho_1$ is the density ratio.

The critical condition to have a stationary wave can be derived by setting $C = 0$ in (3):

$$\frac{Q_1^2}{g'H^3} + \frac{Q_2^2}{g'(D-H)^3} = 1, \quad (4)$$

where H is the critical depth, i.e., the lower layer depth which gives zero wave speed.

This condition can be written in Froude numbers (Mehrotra, 1973 and Armi, 1986):

$$F_1^2 + F_2^2 = 1, \quad (5)$$

where

$$F_1 = U_1/\sqrt{g'H} \qquad F_2 = U_2/\sqrt{g'(D-H)}.$$

Following (3), for given Q_1, Q_2, and D, the inviscid linear wave speed in the two-layer system only varies with lower layer depth "H". The variation of wave speed with lower layer depth is shown in Fig. 2. The thin solid curve represents wave speed in a single layer shallow water flow. Wave speed in a single layer flow decreases monotonically with increasing flow depth. Therefore, if the upstream state is supercritical, a positive perturbation can always be found to allow flow at the trailing edge to be subcritical. As is well

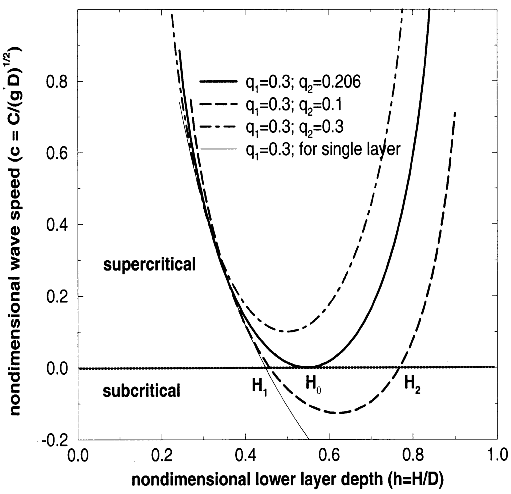

Fig. 2. Plot of the inviscid linear wave speed (C) versus the lower layer depth (H) (3). When $C > 0$, the flow is supercritical, and when $C < 0$ the flow is subcritical. For a two-layer hydrostatic flow, three cases are shown (solid curve) corresponding to different values of the non-dimensional mass flux (43). The dashed curve shows the wave speed of a single layer hydrostatic flow for comparison.

known, a supercritical single layer flow always has a conjugate state.

For two layer flow defined by Q_1, Q_2, and D, there are three different cases (Fig. 2). In the first case, the wave speed curve intercepts the zero wave speed line at two points H_1 and H_2. Part of the wave speed curve lies below the zero speed line, which suggests that there is a range of "H" ($H_1 < H < H_2$), which allows the final-state flow to be subcritical. For this type of flow, if the upstream flow is supercritical, the wave steepening conditions is satisfied.

If the depth of the upstream flow is small ($H < H_1$), a positive perturbation is required to bring the flow into the subcritical regime. Therefore, a hydraulic jump is possible. For a hydraulic jump, the critical depth $H_c = H_1$. The slope dC/dH at the critical depth is negative, so from (3)

$$\frac{Q_1^2}{H_c^4} - \frac{Q_2^2}{(D-H_c)^4} > 0. \tag{6}$$

If the depth of the upstream flow is large, a negative perturbation can steepen and form a hydraulic drop. For a hydraulic drop, the critical depth $H_c = H_2$. The slope at the critical depth is positive, i.e.,

$$\frac{Q_1^2}{H_c^4} - \frac{Q_2^2}{(D-H_c)^4} < 0. \tag{7}$$

A flow with depth between H_1 and H_2 is subcritical, and no steepening is possible.

In the second case, the entire wave speed curve sits above the zero speed line, indicating that a subcritical state can not be achieved by changing the layer depths. Therefore, no perturbation, positive or negative, can alter the flow into a subcritical state. No steady shock can exist.

The marginal case arises when the wave speed curve is tangent to the zero line. The necessary condition for a finite amplitude wave to steepen and form a shock can be derived by evaluating the flow depth of the marginal case.

For a marginal case, H_1 and H_2 merge to H_0 (Fig. 2), i.e., $H_1 = H_2 = H_0 = H_c$. We obtain from (6 and 7)

$$\frac{Q_1^2}{H^4} - \frac{Q_2^2}{(D-H)^4} = 0, \tag{8}$$

or

$$H_0 = \frac{D\sqrt{Q_1}}{\sqrt{Q_1} + \sqrt{Q_2}}. \tag{9}$$

Substituting (9) into (4), we obtain the necessary condition for finite amplitude wave steepening:

$$\sqrt{Q_1} + \sqrt{Q_2} \leqslant (g'D^3)^{1/4}, \tag{10}$$

or

$$\sqrt{F_1} H^{3/4} + \sqrt{F_2}(D-H)^{3/4} \leqslant D^{3/4}, \tag{11}$$

or in non-dimensional form

$$\sqrt{F_1} h^{3/4} + \sqrt{F_2}(1-h)^{3/4} \leqslant 1, \tag{12}$$

where $h = H/D$ is the non-dimensional lower layer depth.

For $h = 0.5$, a regime diagram is constructed (Fig. 3) based on the critical condition (5) and the marginal condition (12). The marginal curve is tangent to the critical curve and divides the super-

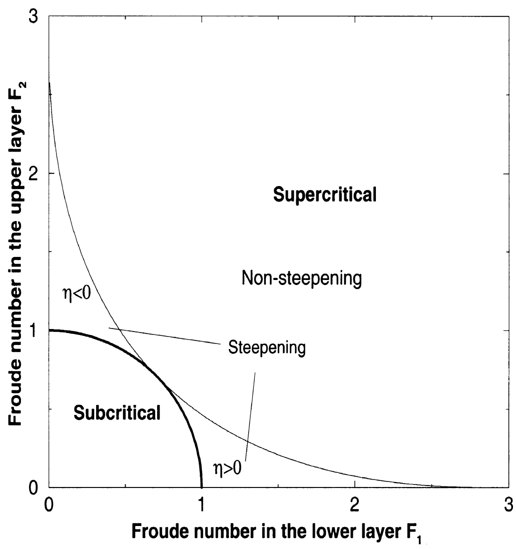

Fig. 3. Wave-steepening diagram. Axes are the two Froude numbers. The critical curve (5) in bold separates the diagram into subcritical and supercritical regimes. The marginal curve (thin solid, based on (12)) with $h =$ 0.5 further divides the supercritical regime into three sub-regimes: steepening for jumps, steepening for drops, and non-steepening. States in the supercritical non-steepening regime have no mass conserving subcritical conjugate states. As seen, steepening requires that one layer be considerably faster and/or thinner than the other layer.

critical region into three regimes. In the jump regime, there are values of $\eta > 0$ satisfying $C_b \leqslant 0$. In the drop regime, there are negative η values satisfying $C_b \leqslant 0$. And in the "non-steepening" regime, no values of η exist for which $C_b \leqslant 0$. On a $F_1 \times F_2$ diagram, the marginal curve (12) is a function of flow depth h. These regimes can be equally well defined on a mass flux $(Q_1 \times Q_2)$ diagram, on which the marginal curve is a universal curve and the critical curve becomes h-dependent. For strongly asymmetric flows, the wave steepening condition may be satisfied for supercritical flows as the jump $(\eta > 0)$ or drop $(\eta < 0)$ modified flow may have an increased linear wave speed. For nearly symmetric flows, $F_1 \simeq F_2$, and $h \simeq 0.5$, the steepening tendency is absent and no value of η can satisfy $C_b = 0$. No steady shocks can exist in this situation.

If $Q_2 = 0$, the critical curve (5) reduces to $F_1 = 1$, and the marginal curve (12) reduces to $F_1 < h^{-3/2}$, the proper limit for two layer flow under a rigid lid with the upper layer at rest. With a deep upper layer (i.e., $D \to \infty$ and $h \to 0$), the 2-layer system reduces to a single layer flow, and the steepening condition $F_1 < \infty$ is always satisfied.

3. The formulation of ideal shock theory

While the constraint imposed and the intuition provided by steepening theory are useful, there is still a need for a more complete shock theory. First, steepening theory gives only a necessary condition (12), but does not guarantee shock existence. Second, a complete shock theory would provide more information about the end-state of a shock, including Bernoulli losses.

Traditionally, analysts tried to predict the shock end-state state directly, using conservation laws and closure assumptions. While this approach is fine for a one-layer system, the post-shock state in two- and multi-layer systems depends on the momentum transport between layers by pressure forces. This requires that we derive a self-consistent model equation describing internal shock structure.

We consider a two layer Boussinesq flow under a rigid lid, and assume that the flow is steady relative to the shock. The pre- and post-shock flow is uniform within each layer and without viscous stresses. Flow within the shock is nearly uniform vertically and has viscous stresses. These viscous stresses are mostly normal stresses, with higher order shear stresses associated with the tilted stress-free interface. We can still define the mass flux as (1–2).

In a steady shock with free slip boundary conditions along the flat bottom, the rigid lid, and the interface, the vertically integrated momentum equations can be written as (SS95)

$$\frac{\mathrm{d}}{\mathrm{d}x}\left(\frac{Q_1^2}{H} + rgHD - rgH^2 + \frac{1}{2}gH^2 + PH\right) = f_{1x} + PH_x + rg(D-H)H_x, \tag{13}$$

$$\frac{\mathrm{d}}{\mathrm{d}x}\left(\frac{Q_2^2}{D-H} + \frac{1}{2}gD^2 + \frac{1}{2}gH^2 - gDH + PD - PH\right) = f_{2x} - PH_x - g(D-H)H_x, \tag{14}$$

where $r = \rho_2/\rho_1$ is the density ratio, P is the pressure along the rigid top, and f_{1x} and f_{2x} are dissipative terms. According to SS93 and SS95 (also see Gustafsson and Sundstrom, 1978), the vertically integrated viscous force can be written as

$$f_1 = Hv_1\left(\frac{Q_1}{H}\right)_x, \tag{15}$$

$$f_2 = (D-H)v_2\left(\frac{Q_2}{D-H}\right)_x, \tag{16}$$

where v_1, and v_2 are viscous coefficients. The final terms (in (13) and (14)) represent the momentum exchange along the interface due to the hydrostatic pressure force.

Eliminating P from eqs. (13) and (14), we obtain:

$$\left(1 - \frac{Q_1^2}{g'H^3} - \frac{Q_2^2 H}{g'(D-H)^3}\right)H_x = -\frac{Q_1}{g'H}\frac{\mathrm{d}}{\mathrm{d}x}\left(v_1\frac{H_x}{H}\right) - \frac{Q_2}{g'(D-H)}\frac{\mathrm{d}}{\mathrm{d}x}\left(v_2\frac{H_x}{D-H}\right), \tag{17}$$

where $g' = (\rho_1 - \rho_2)g/\rho_1$ is the reduced gravity.

We consider two viscous formulations, Newtonian and non-Newtonian, in order to determine the sensitivity of macroscopic shock behavior to the way that viscous processes are treated.

Newtonian fluids:

$$v_1 = \alpha_1, \quad v_2 = \alpha_2; \tag{18}$$

non-Newtonian fluids:

$$v_1 = \beta_1 |U_{1x}|, \quad v_2 = \beta_2 |U_{2x}|, \tag{19}$$

where α_1, α_2, β_1, and β_2 are constants. For non-Newtonian fluids (19), the viscosity (v_i) is assumed to be proportional to its corresponding strain-rate ($|U_{ix}|$, e.g., Smith, 1977). Eq. (17) is a second order, nonlinear, ordinary differential equation for $H(x)$.

4. Weak shock solution

For a weak shock, we can reduce (17) to a simpler equation by expanding it about the critical state H_c and collecting the lowest order terms. Using $H = H_c + \eta$, for a weak shock, we have $|\eta| \ll H_c$. Dropping the higher order terms in η, for Newtonian fluids, we obtain:

$$3\left(\frac{Q_1^2}{H_c^4} - \frac{Q_2^2}{(D-H_c)^4}\right)\eta\eta_x = -\left(\alpha_1 \frac{Q_1}{H_c^2} + \alpha_2 \frac{Q_2}{(D-H_c)^2}\right)\eta_{xx}, \tag{20}$$

while for non-Newtonian fluids, we obtain

$$3\left(\frac{Q_1^2}{H_c^4)} - \frac{Q_2^2}{(D-H_c)^4}\right)\eta\eta_x = -2\left(\beta_1 \frac{Q_1^2}{H_c^4} + \beta_2 \frac{Q_2^2}{(D-H_c)^4}\right)|\eta_x|\eta_{xx}. \tag{21}$$

To simplify eqs. (20) and (21), we define a horizontal length scale as

$$L_n = \frac{\alpha}{3\eta_0} \frac{Q_1/H_c^2 + \gamma_n Q_2/(D-H_c)^2}{Q_1^2/H_c^4 - Q_2^2/(D-H_c)^4} \tag{22}$$

for Newtonian fluids, and

$$L_{nn} = \sqrt{\frac{2\beta}{3} \frac{Q_1^2/H_c^4 + \gamma_{nn} Q_2^2/(D-H_c)^4}{Q_1^2/H_c^4 - Q_2^2/(D-H_c)^4}} \tag{23}$$

for non-Newtonian fluids, where η_0 is the upstream value of η, $\alpha_2 = \gamma_n \alpha_1 = \gamma_n \alpha$, and $\beta_2 = \gamma_{nn}\beta_1 = \gamma_{nn}\beta$. Using $\hat{x} = x/L_n$, eq. (20) can be written as

$$\eta_{\hat{x}\hat{x}} = -2\eta\eta_{\hat{x}}. \tag{24}$$

Using $\hat{x} = x/L_{nn}$, eq. (21) can be written as

$$\eta = -\mathrm{sgn}(\eta_{\hat{x}})\eta_{\hat{x}\hat{x}}. \tag{25}$$

The monotonic solutions to eqs. (10) and (11) are (SS95),

$$\eta(\hat{x}) = \eta_0 \tanh(\hat{x}), \tag{26}$$

$$\eta(\hat{x}) = \left\{\begin{matrix} -\eta_0 & \text{for } \hat{x} < -\pi/2 \\ \eta_0 \sin(\hat{x}) & -\pi/2 < x < \pi/2 \\ \eta_0 & \text{for } \hat{x} > \pi/2 \end{matrix}\right\}. \tag{27}$$

For Newtonian fluids, the length scale (22) is determined by a balance between the nonlinear steepening effect and the dissipation effect. The stronger the shock (i.e., η_0 larger), the narrower the shock. On the other hand, the viscosity (α in (22) and β in (23)) resists this "narrowing" tendency and makes the shock broader.

For non-Newtonian fluids, the strain-rate in the viscous term cancels with the interface slope in the nonlinear steepening term. The equation representing a balance between steepening and viscosity variation reduces to a linear eq. (25). The length scale (23) is proportional to the square root of the viscosity coefficient β.

To have the length scale L_n or L_{nn} positive, for both Newtonian fluids (22) and non-Newtonian fluids (23), requires

$$\eta_0\left(\frac{Q_1^2}{H_c^4} - \frac{Q_2^2}{(D-H_c)^4}\right) > 0. \tag{28}$$

Or for a hydraulic jump ($\eta_0 > 0$)

$$\frac{Q_1^2}{H_c^4} - \frac{Q_2^2}{(D-H_c)^4} > 0, \tag{29}$$

and for a hydraulic drop ($\eta_0 < 0$),

$$\frac{Q_1^2}{H_c^4} - \frac{Q_2^2}{(D-H_c)^4} < 0. \tag{30}$$

Conditions (29) and (30) are identical to the steepening conditions (6) or (7) derived in Section 2. Therefore, length-scales L_n and L_{nn} are always positive for allowable pre-shock states.

The Bernoulli changes in each layer can be computed by integrating the dissipative force across the internal shock along an average streamline, i.e.

$$\Delta B_1 = \int_a^b \frac{f_{1x}}{H}\,\mathrm{d}x = \int_a^b (v_1 U_{1x})_x\,\mathrm{d}x + \int_a^b \frac{v_1 U_{1x} H_x}{H}\,\mathrm{d}x, \quad (31)$$

$$\Delta B_2 = \int_a^b \frac{f_{2x}}{D-H}\,\mathrm{d}x = \int_a^b (v_2 U_{2x})_x\,\mathrm{d}x + \int_a^b \frac{v_2 U_{2x}(D-H)_x}{D-H}\,\mathrm{d}x. \quad (32)$$

Noticing that the first terms in (31) and (32) are in flux form and their integrals are zero, we obtain

$$\Delta B_1 = \int_a^b \frac{v_1 U_{1x} H_x}{H}\,\mathrm{d}x, \quad (33)$$

$$\Delta B_2 = \int_a^b \frac{v_2 U_{2x}(D-H)_x}{D-H}\,\mathrm{d}x \quad (34)$$

To the lowest order, (33) and (34) are

$$\Delta B_1 = \frac{Q_1}{H_\mathrm{c}^3}\int_a^b v_1(\eta_x)^2\,\mathrm{d}x + \text{h.o.t.}, \quad (35)$$

$$\Delta B_2 = \frac{Q_2}{(D-H_\mathrm{c})^3}\int_a^b v_2(\eta_x)^2\,\mathrm{d}x + \text{h.o.t.}. \quad (36)$$

A derivation of (31–36) can be found in Section 9.

Using (26) in (35) and (36), we obtain for Newtonian fluids:

$$\Delta B_1 = -Q_1 \frac{Q_1^2/H_\mathrm{c}^4 - Q_2^2/(D-H_\mathrm{c})^4}{Q_1/H_\mathrm{c}^2 + \gamma_n Q_2/(D-H_\mathrm{c})^2}\,\frac{\varepsilon^3}{4}, \quad (37)$$

$$\Delta B_2 = -Q_2\gamma_n\left(\frac{H_\mathrm{c}}{D-H_\mathrm{c}}\right)^3 \times \frac{Q_1^2/H_\mathrm{c}^4 - Q_2^2/(D-H_\mathrm{c})^4}{Q_1/H_\mathrm{c}^2 + \gamma_n Q_2/(D-H_\mathrm{c})^2}\,\frac{\varepsilon^3}{4}, \quad (38)$$

where $\varepsilon = (\eta_1 - \eta_0)/H_\mathrm{c}$, is a measure of shock strength, andη_1 is the post-shock value of η. As in one-layer shocks, the Bernoulli drop is proportional to the cube of the shock strength (ε).

Similarly, for non-Newtonian fluids, we obtain (from 27, 35, and 36)

$$\Delta B_1 = -\frac{Q_1^2}{H_\mathrm{c}^2}\,\frac{Q_1^2/H_\mathrm{c}^4 - Q_2^2/(D-H_\mathrm{c})^4}{Q_1^2/H_\mathrm{c}^4 + \gamma_{nn} Q_2^2/(D-H_\mathrm{c})^4}\,\frac{\varepsilon^3}{4}, \quad (39)$$

$$\Delta B_2 = -\frac{\gamma_{nn}Q_2^2}{(D-H_\mathrm{c})^2}\left(\frac{H_\mathrm{c}}{D-H_\mathrm{c}}\right)^3 \times \frac{Q_1^2/H_\mathrm{c}^4 - Q_2^2/(D-H_\mathrm{c})^4}{Q_1^2/H_\mathrm{c}^4 + \gamma_{nn} Q_2^2/(D-H_\mathrm{c})^4}\,\frac{\varepsilon^3}{4}. \quad (40)$$

Note that while the Bernoulli drops are third-order quantities, we have been able to compute them from the first order solutions. The Bernoulli changes for both Newtonian (37 and 38) and non-Newtonian (39 and 40) fluids have the correct forms in both the vanishing amplitude limit and single layer limit. As $\varepsilon \to 0$, from (37), (38), (39), and (40), we have $\Delta B_1 = \Delta B_2 = 0$. If $Q_2 = 0$, the internal shock reduces to a single layer jump. The Bernoulli changes can be written as $\Delta B_1/(g'H_\mathrm{c}) = -\varepsilon^3/4$ and $\Delta B_2 = 0$, which agrees with the classical shock solution for a weak single layer shock (SS95). If $Q_1 = 0$, the Bernoulli changes reduce to $\Delta B_1 = 0$, $\Delta B_2/[g'(D-H_\mathrm{c})] = -\varepsilon^3/4$.

For both hydraulic jumps ($\varepsilon > 0$) and hydraulic drops ($\varepsilon < 0$), eqs. (37), (38), (39), and (40) show that the Bernoulli changes in both layers are negative. Therefore, for a viscous internal shock with two active layers ($Q_1 \neq 0$ and $Q_2 \neq 0$), the entropy principle is valid in each layer. Eqs. (37–40) also imply that the Bernoulli changes in both layers are independent of the viscous coefficients α or β.

Another remarkable feature is that for both Newtonian flow and non-Newtonian flow, the Bernoulli changes show explicit dependence on the viscous ratio γ_n or γ_{nn}. The value of γ_n or γ_{nn} could be considered either as a physical property of the fluid or a quantity related to the turbulent nature of flow in the shock. Because of the one-to-one relation between Bernoulli changes and the final post-shock state, this result suggests that the post-state can not be precisely determined by its pre-shock state. The fluid property or its turbulent nature may influence the conjugate state for a given pre-shock state.

For Newtonian fluids, the ratio of Bernoulli changes can be expressed as

$$\frac{\Delta B_1}{\Delta B_2} = \frac{Q_1}{\gamma_n Q_2}\left(\frac{D-H_\mathrm{c}}{H_\mathrm{c}}\right)^3, \quad (41)$$

using (37) and (38). According to (41), the ratio of Bernoulli losses in the 2 layers is inversely proportional to the third power of the ratio of critical flow depths. This is so because that the Bernoulli loss in a layer is proportional to the cube of the relative depth change (η/H) for Newtonian fluids (SS95). While, the depth change η has the same magnitude in both layers, the relative depth change, the viscous forces and the resulting Bernoulli loss are stronger in the thinner layer. For a typical shock, the thinner layer has a tendency to expand. Therefore, assuming $\gamma_n \sim 1$, eq. (41) implies that the Bernoulli loss is much larger in the expanding layer.

For non-Newtonian flow, the ratio of Bernoulli changes can be expressed as

$$\frac{\Delta B_1}{\Delta B_2} = \frac{1}{\gamma_{nn}} \left(\frac{Q_1}{Q_2}\right)^2 \left(\frac{D - H_c}{H_c}\right)^5. \tag{42}$$

Similarly, with $\gamma_{nn} \sim 1$, eq. (42) implies a relatively stronger dissipation in the expanding layer. This suggests that for both Newtonian fluids and non-Newtonian fluids, after a dissipative internal shock, the Bernoulli loss in the contracting layer is smaller than that in the expanding layer. The concentration of Bernoulli loss in the expanding layers agrees with most previous work (e.g., WS84) but disagrees with the strong bore results of KRS97 due to the mixing of momentum between layers in that case.

The role of the viscosity ratio γ in determining the Bernoulli change ratio (41, 42) can be understood as follows. If both layer viscosities increase, the shock widens and the Bernoulli losses are unchanged. If just one viscosity increases, the shock still widens a little to reach a new balance with the non-linear steepening tendency. The Bernoulli loss of the more viscous layer increases as that layer plays a larger rôle in preventing nonlinear steepening. The increased width decreases the viscous stresses in the other layer, reducing its Bernoulli loss.

5. Finite shock solutions and Tail modes

5.1. Viscous tail modes

For Newtonian fluids with $v_1 = v_2 = v$, the governing equation for finite amplitude shocks (17) can be written in nondimensional form,

$$\left(1 - \frac{q_1^2}{h^3} - \frac{q_2^2}{(1-h)^3}\right) h_x = -\frac{q_1}{h}\frac{\mathrm{d}}{\mathrm{d}x}\left(\frac{h_x}{h}\right) - \frac{q_2}{1-h}\frac{\mathrm{d}}{\mathrm{d}x}\left(\frac{h_x}{1-h}\right), \tag{43}$$

where $q_{1,2} = Q_{1,2}/(g'^{1/2} D^{3/2})$, $h = H/D$, and $x = x/v$. The absence of v in eq. (43) reflects the pseudoinviscid nature of a viscous shock (SS95).

The nondimensional boundary conditions are

$$h(x = -\infty) = h_a, \qquad h_x(x = -\infty) = 0, \qquad h_x(x = \infty) = 0, \tag{44}$$

where $h_a = H_a/D$ is the nondimensional pre-shock flow depth.

Even for a shock with a finite amplitude, one can expect that the slope of the interface near the leading or trailing edge is so gentle that eq. (43) can be linearized. Using $h(x) = h_0 + \hat{h}(x)$, and $\hat{h}(x) \ll h_0$, we obtain:

$$\left(1 - \frac{q_1^2}{h_0^3} - \frac{q_2^2}{(1-h_0)^3}\right) \hat{h}_x = -\left(\frac{q_1}{h_0^2} + \frac{q_2}{(1-h_0)^2}\right) \hat{h}_{xx}, \tag{45}$$

where h_0 is the equilibrium depth at the leading/trailing edge.

Eq. (45) has two eigenvalues, i.e., $\lambda = 0$ and:

$$\lambda = \frac{q_1^2/h_0^3 + q_2^2/(1-h_0)^3 - 1}{q_1/h_0^2 + q_2/(1-h_0)^2}. \tag{46}$$

Eigenvalue (46) corresponds to an eigen-mode, $e^{\lambda x}$, which we refer to as a viscous tail mode. The concept of the viscous tail mode is very important as explained below.

First, because x increases along the flow direction, a positive/negative λ implies that either the sloped interface gradually becomes flat and converges towards the upstream/downstream state or that it diverges. Therefore, a physical shock must have a positive λ at its leading edge and a negative λ at its trailing edge so that equilibrium pre-shock/post-shock states can be reached. Comparing (46) with the development in Section 2, indicates that $\lambda > 0$ for supercritical flow and $\lambda < 0$ for subcritical flow. This proves that a two layer Newtonian-viscous shock must correspond to a transition from a supercritical flow to a subcritical flow, as assumed in Section 2. Also the uniqueness of the tail mode provides a unique boundary condition, giving a unique conjugate state for a given pre-shock state.

To numerically solve the quadratic, second order, ordinary differential eq. (43), a critical issue is how to apply the boundary conditions specified at infinity (44). The viscous tail mode concept allows us to start and end the integration at some finite distance from the center of the shock. The full solution can be obtained by matching together the numerical solution of the inner nonlinear part and the analytical solutions of the linear parts near the ends. In practice, this is done by specifying a small initial interface perturbation and computing the corresponding interface slope from the upstream tail eigen-mode. These values are then used to start the integration of the governing equation. When the ratio of perturbation value to slope (λ) reaches that of the downstream tail mode, the integration is ended.

The use of the tail mode concept in proving uniqueness and initializing integrations, which is rather trivial here, becomes much more important in a two layer shock under a upper free surface, as there are two wave modes (Jiang and Smith, 2001).

5.2. *Shock bifurcation and wave steepening*

Using the tail mode method, for a given supercritical flow state specified by F_1, F_2 and h_a, the shock structure and end state can be solved on a finite difference grid. As examples, two sets of solutions are shown in Fig. 4 with $h_a = 0.5$, $F_2 = 0.1$ and $h_a = 1/3$, $F_2 = 0.2$, respectively. The post-shock states (o) predicted by system (43) and (44) are linked to their corresponding pre-shock states (x, specified by F_1, F_2 and h_a) by "shock trajectories". For a given pre-shock state, a unique mass conserving shock trajectory is defined on a Froude number diagram by:

$$F'_1 = F_1(h/h_a)^{1.5},$$
$$F'_2 = F_2(1-h)^{1.5}/(1-h_a)^{1.5}, \tag{47}$$

where h is the local depth of flow in the lower layer. Only the portions within the shock (i.e., $h_a < h < h_b$) are plotted in Fig 4.

The solid curves are the boundaries of shock and non-shock regimes based on the wave steepening argument (Section 2). Fig. 4 suggests that there is an agreement between the finite shock

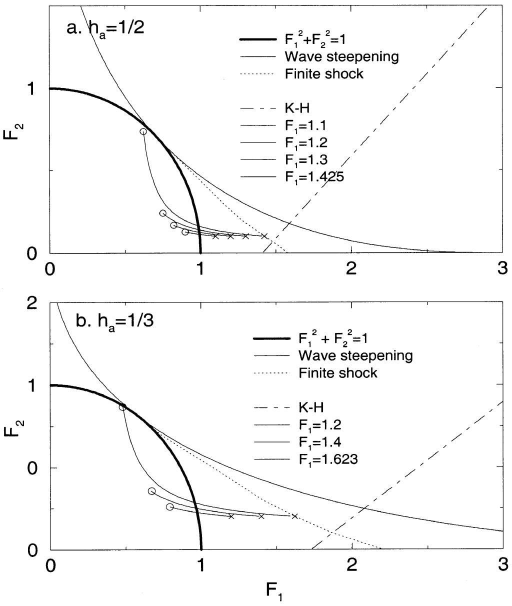

Fig. 4. Examples of finite shock solutions for upstream depth ratios of $h = 1/2$ and $1/3$. The bold solid curve is the critical curve (5). The thin solid curve is the marginal curve (12). The dotted curve is the limit of shock existence according to ideal shock theory with a Newtonian viscous formulation. The dashed-dotted line represent the shear instability boundary (57). Two sets of solutions are shown: (a) $h_a = 0.5$, $F_2 = 0.1$ and $F_1 = 1.1$, 1.2, 1.3, 1.425; (b) $h_a = 1/3$, $F_2 = 0.2$ and $F_1 = 1.2$, 1.4, 1.623. The symbol "×" represents a pre-shock state, and "○" represents a post-shock state.

solutions and the wave steepening theory in the sense that the viscous shock solutions show proper pre-shock and post-shock states, i.e., all pre-shock states are in the supercritical jump regime and all post-shock states are in the subcritical regime.

However, a mathematical bifurcation occurs at pre-shock points still in the supercritical jump regime (e.g., $F_1 = 1.425$, $F_2 = 0.1$, $h_a = 0.5$ and $F_1 = 1.623$, $F_2 = 0.2$, $h_a = 1/3$). Beyond these points (i.e., for a larger F_1), the numerical solution nearly approaches a constant downstream state, but then diverges. This divergence indicates that $\lambda_b > 0$. Indeed, we see in Fig. 4 that as the pre-shock states approach the bifurcation curve, the end states reach the critical curve and pass back into the supercritical regime. Thus, the steepening condition is violated. To represent this graphically, a second marginal curve, marking the occurrence of the bifurcation, is shown dotted. Values for plotting this curve were derived numerically for a set of h_a values. A similar curve could be plotted in the drop regime.

The existence of the second marginal curve reminds us that the wave steepening theory (Section 2) only provides a necessary condition for shocks. It required only that a subcritical end-state exist within a mass conservation constraint. It did not require that a subcritical end-state be "accessible" by the full viscous governing equations. Viscous shock theory is more complete as it gives the sufficient condition to have a steady shock.

5.3. *Bernoulli loss*

The determination of the precise post-shock states with a numerical integration allows us to compute the Bernoulli loss in the traditional way, i.e., $\Delta B_i = B_{ib} - B_{ia}$. The cube roots of the Bernoulli losses in both layers are plotted as a function of F_1 for both cases $h_a = 0.5$, $F_2 = 0.1$ and $h_a = 1/3$, $F_2 = 0.2$. The corresponding weak shock predictions based on (37) and (38) are plotted for comparison.

Fig. 5 shows that there are Bernoulli drops in both layers, which increase with shock strength (i.e., F_1). For both cases, the Bernoulli drop in the lower (expanding) layer is larger than that in the upper (contracting) layer, which agrees with experimental observations (WS84). The weak shock solutions follow the finite shock solutions well to about $F_1 = 1.2$. For stronger shocks, the weak shock solutions have a tendency to underestimate the Bernoulli drop in both layers.

The agreement between the finite amplitude shock theory and the weak shock prediction suggests that the calculation of Bernoulli change by integrating the viscous force across a shock (33, 34) is equivalent to the conventional method (i.e., taking the Bernoulli difference between the post-shock and the pre-shock state).

The curve in Fig. 5 describing the Bernoulli drop from numerical integrations is extended beyond the bifurcation point along the x-axis, to remind the reader that no shock is possible beyond that point. The dots and circles representing the shallow water model simulations will be discussed in the next section.

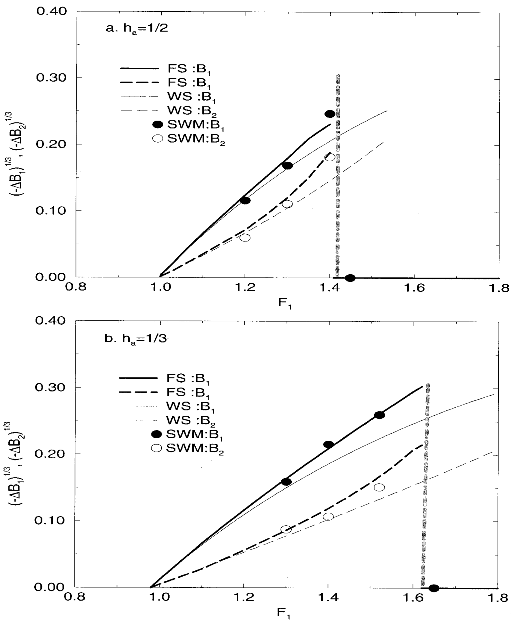

Fig. 5. Cubic roots of the Bernoulli losses in two layer shocks using the finite amplitude shock equation and the weak shock solution. FS: finite amplitude shock solution for Newtonian fluids based on nine runs (in bold); WS: weak shock solution for Newtonian fluids (37, 38); SWM: shallow water model predictions; The bold dashed line represents the position of the numerical bifurcation. (a) $h_a = 0.5$, $F_2 = 0.1$; (b) $h_a = 1/3$, $F_2 = 0.2$.

6. Flow over an obstacle

As a classical fluid dynamical problem, layered flow over an obstacle has been studied extensively over the last fifty years (Long, 1954; 1970; 1974; Houghton and Kasahara, 1968; Houghton and Issacson, 1968; Baines and Davies, 1980; Baines, 1984; Pratt, 1983; and KRS97 among others). More recently, these investigations have been extended to two horizontal dimensions, using a numerical shallow water model (i.e., SWM) to simulate atmospheric flow beneath a low level inversion. Some significant agreement has been found between observations and this type of model predictions, such as the quasi-stationary eddies downstream of Hawaii (Grubišić et al., 1995), the long wake behind St. Vincent (Smith et al., 1997), and the gap wind structure near the Aleutian Islands (Pan and Smith, 1999).

Our motivation in this section, is to see whether the shocks which form in simple numerical shallow water models have characteristics which are similar to those predicted by ideal shock theory. As we will see, a useful comparison can be made by examining bow shocks ahead of an obstacle in supercritical flow.

6.1. *The numerical shallow water model*

Traditional schemes of shallow water model formulation either conserve total energy or total potential enstrophy, or both (Sadournay, 1975; Haltiner and Williams, 1980; and Arakawa and Lamb, 1981). These schemes are often used in isentropic/isopycnic atmosphere/ocean models due to their attractive stability properties. However, it is inappropriate to use this type of formulation to simulate hydraulic jump related processes, where dissipation can be significant. Instead, we use a mass and momentum conserving formulation (SS93).

In the absence of bottom friction and ambient rotation, the governing equations for a two layer Boussinesq flow under a upper free surface are

$$\frac{\mathrm{D}\boldsymbol{V}_1}{\mathrm{D}t} + g\nabla(h_1 + rh_2 + h) = 0, \tag{48}$$

$$\frac{\mathrm{D}\boldsymbol{V}_2}{\mathrm{D}t} + g\nabla(h_1 + h_2 + h) = 0. \tag{49}$$

$$\frac{\mathrm{D}h_i}{\mathrm{D}t} + h_i\nabla\cdot\boldsymbol{V}_i = 0, \tag{50}$$

where $\boldsymbol{V}_i = (u_i, v_i)$ is the horizontal velocity, g is the gravity, h_i is the depth of the fluid layer and h refers to the elevation of the bottom topography, ρ_i is the density, r is the density ratio $(=\rho_2/\rho_1)$ and the index $i = 1, 2$ refers to the lower layer and upper layer, respectively.

The topography is a circular Gaussian shaped bump, which is described analytically by

$$h(x, y) = h_m \exp[-(x^2 + y^2)/a^2], \tag{51}$$

where a is the radius of the bump.

We non-dimensionalize eqs. (48), (49), (50), and (51) using the following scales: The reference depth H_∞ for the vertical length scale, topography radius a for the horizontal length scale, $\sqrt{gH_\infty}$ for the horizontal velocity scale and $a/\sqrt{gH_\infty}$ for the time scale.

The resulting non-dimensional version of eqs. (48–50) become

$$\frac{\mathrm{D}\boldsymbol{V}_1}{\mathrm{D}t} + \nabla(h_1 + rh_2 + h) = 0, \tag{52}$$

$$\frac{\mathrm{D}\boldsymbol{V}_2}{\mathrm{D}t} + \nabla(h_1 + h_2 + h) = 0, \tag{53}$$

$$\frac{\mathrm{D}h_i}{\mathrm{D}t} + h_i\nabla\cdot\boldsymbol{V}_i = 0. \tag{54}$$

The non-dimensional Bernoulli functions along the bottom and the interface are defined as

$$B_1 = \frac{1}{2}\boldsymbol{V}_1\cdot\boldsymbol{V}_1 + h + h_1 + rh_2, \tag{55}$$

$$B_2 = \frac{1}{2}\boldsymbol{V}_2\cdot\boldsymbol{V}_2 + h + h_1 + h_2, \tag{56}$$

where B_1 and B_2 was scaled by gH_∞.

The model for this study was coded based on the momentum eqs. (52–53) in flux form (Schär and Smith, 1993; Schär and Smolarkiewicz, 1996). This formulation conserves total momentum and allows energy dissipation and enstrophy generation at regions where hydraulic jumps occur. No mixing across the interfaces is allowed, even in jumps. The neglect of mixing is consistent with the assumption of our ideal shock theory.

A somewhat similar formulation was used by Houghton and Kasahara (1968) and Houghton and Issacson (1968). Their scheme conserves energy through most of the domain except in hydraulic jump regions where YG's jump condition was explicitly used to match the flow upstream and downstream of the jump.

To make the model comparable to the theory we developed in the previous sections (i.e., two layer Boussinesq flow with an upper rigid lid), we chose a large density ratio $r = 0.95$. In this case, for slow flows (similar to the internal wave speed), the upper free surface remains nearly flat, simulating a rigid lid. The justification of using a free surface model and the rescaling details are discussed in Section 10.

A relaxation boundary condition has been used to reduce the influence of the reflection of the external wave mode. A large domain is chosen with 800×400 grid points, and the 8 grid points near the boundaries are dedicated to the relaxation zone. The spatial resolution for this example is $DX = DY = 0.1$. To make the model stable, the corresponding temporal resolution is $DT = 0.025$.

Weak lateral friction is added for the purpose of smoothing the fields (SS93).

6.2. Simulations

In this sub-section, we compare the SWM simulations with ideal shock theory. In order to do this most conveniently, we select an isolated obstacle in supercritical flow, and focus our attention on the bow shock which forms just ahead of the obstacle (Jiang and Smith, 2000). The advantage of a bow shock is that its pre-shock state is very nearly the flow imposed at the upstream boundary of the domain. Unlike 1-D flow, where bow shocks usually propagate away to upstream infinity, in 2-D flow, the bow shock finds a stable steady position. On the centerline, the shock is normal to the flow. This normal shock can be directly compared with our ideal shock theory, as long as the bow shock is not highly curved, that is, the shock thickness should be much less than the radius of curvature of the shock.

In practice, care must be taken to integrate to a good steady state. Even a slight drift of the bow shock position can give inaccurate Bernoulli drop values, unless one shifts to a coordinate system moving with the shock. As discussed below, one other issue can arise; shear instability. As acceptable two-layer pre-shock states are often vertically sheared, care must be taken not to specify a shear so large that shear instability occurs.

For $h_a = 0.5$, $F_2 = 0.1$, $r = 0.95$, and $M = 0.35$, 4 successful runs were carried out to steady states. These runs corresponded to $F_1 = 1.2$, 1.3, 1.4, and 1.43 respectively. For the first three of these cases, a steady bow shock formed in front of the obstacle (Fig. 6). A pair of trailing V-waves appear in the lee side (JS99a). Although there is a sharp rise along the lower interface, the upper free surface is almost unchanged indicating that the free surface is acting like a rigid lid. The total integration time T varied for each case. In nondimensional time units, for $F_1 = 1.4$, $T = 300$, for $F_1 = 1.3$, $T = 400$, and for $F_1 = 1.2$, $T = 500$. As the flow approaches the critical curve, and the steepening tendency weakens, it takes a longer time to reach a steady state. Theoretically, for points on the critical curve, no steady state can be achieved. For a weakly supercritical flow (e.g., $F_1 = 1.2$, 1.3), the bow-shock is far upstream of the obstacle so that the pre-shock flow is approximately the same as the unperturbed flow. For the stronger supercritical flow, the bow shock sits on the upstream slope of the obstacle, and the pre-shock state is slightly modified by the underlying terrain. The cubic roots of the Bernoulli drop in the lower layer and upper layer along the center streamline are plotted (as circles and dots) in Fig 5a as a function of the pre-shock F_1. The fourth run had $F_1 = 1.43$. No bow shock was found.

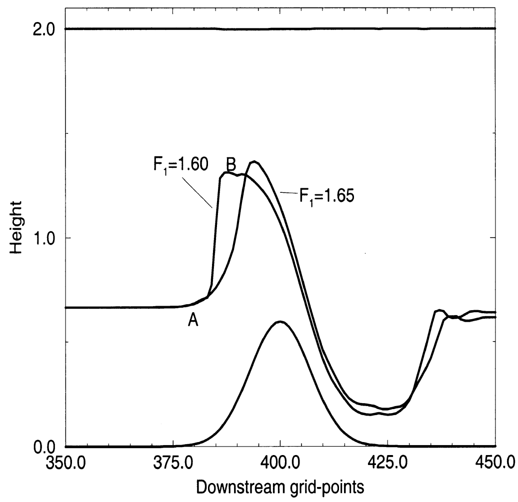

Fig. 6. The cross section along the centerline of two SWM simulations of 2-D, 2-layer flow over an isolated bump. The upstream conditions are $F_1 = 1.6$ and 1.65, $F_2 = 0.2$, $H_1 = 0.6667$, $H_2 = 1.3333$, and $r = 0.95$, which gives $h_a = 1/3$. The fluid interfaces are shown. For the case $F_1 = 1.6$, a well defined bow-shock appears between A and B with a Bernoulli drop (Fig. 5b). For the case $F_1 = 1.65$, no shock forms.

There is a surprisingly good agreement between the SWM runs and the ideal shock theories. The agreement has two aspects. First, there is a satisfactory quantitative agreement between the ΔB from SWM simulations and the finite amplitude shock solutions. Secondly, at the ambient flow Froude number of $F_1 = 1.43$ (the bold dashed line in Fig. 5), a bifurcation occurs in the SWM simulations, i.e., beyond this value, no bow-shocks can form and the Bernoulli drop upstream of the obstacle becomes indiscernible. It is interesting that this bifurcation point is approximately the same as predicted by finite amplitude shock theory. However, as indicated in Fig 4, the bifurcation point for $h_a = 0.5$ and $F_2 = 0.1$ is very close to the shear instability regime. For the last point shown ($F_1 = 1.45$), although it is clear that there is no bow-shock in the upstream side, shear instability induced noise was observed in the computed domain.

As is well known, with strong vertical shear across an infinitesimally thin interface, shear instability may occur in a two layer flow system. With the Boussinesq approximation, the shear instability criterion for two layer rigid lid hydrostatic flow is (Baines, 1995):

$$\frac{|U_1 - U_2|}{\sqrt{g'D}} > 1; \tag{57}$$

for $h_a = 0.5$ and $h_a = 1/3$, (57) is plotted on Fig. 4 as dashed lines.

To reduce the unwanted influence of shear instability, a second set of runs with $h_a = 1/3$, $F_2 = 0.2$, $r = 0.95$, and $M = 0.35$ were carried out (Fig. 5b). Under these conditions, the shock marginal curve and the shear instability curve are further apart. A similar agreement was found between the SWM simulations and the finite amplitude shock solutions. For $F_1 = 1.6$, the pre-shock state is modified by the underlying terrain to $F_1 = 1.52$ and a clear bow shock is found. However, no bow-shock is found in the run with $F_1 = 1.65$. The bifurcation found in the first set of runs is thereby verified. Further numerical simulations suggest that these bifurcation points are quite robust. They are not sensitive to the mountain height.

The flow depths along the center streamline for the ambient Froude numbers $F_1 = 1.6$ and $F_1 = 1.65$ are shown in Fig. 6. For $F_1 = 1.6$, there is a well defined bow-shock between points A and B. For $F_1 = 1.65$, no bow-shock forms and the Bernoulli drop on the upstream slope is zero.

The rather remarkable agreement between ideal shock theory and the SWM is somewhat curious. Paradoxically, the ideal shock theory indicates that the viscous formulation may play some role in shocks, yet the SWM has no explicit viscous formulation at all! Dissipative fluxes must arise implicitly from the finite difference coding. We note however that the theoretically predicted influence of the viscous formulation is rather weak and the numerical dissipation may approximately fit the Newtonian and equal-layer-viscosity assumption used in Fig. 5.

7. Discussion

In this paper, we developed a theory of ideal shocks in two fluid layers under a rigid lid. By our definition, an ideal shock satisfies three assumptions: (1) hydrostatic flow inside the shock, (2) a viscous behavior for dissipation in the shocks, (3) no mixing of momentum or buoyancy across the interface. The results of the analysis include a shock regime diagram, formulae for Bernoulli loss, uniqueness conditions and a prediction of shock bifurcation.

As a first step, we determined an approximate shock regime diagram which follows from the steepening hypothesis: i.e., that any shock must start in a supercritical state and have a range of accessible mass-conserving sub-critical states. Closed form expressions for the critical and marginal curves are derived which divide the regime diagram into four segments; one subcritical regime and three supercritical regimes; jump, drop and no-shock. Two-layer shocks (i.e., jumps or drops) can form only in supercritical flow and only when one layer is sufficiently thinner and/or faster than the other layer.

In Section 3, a steady state non-linear viscous shock equation is derived. The non-dimensional form of this equation demonstrates the pseudo-inviscid nature of ideal shocks; i.e., that the width scale, but not the shock profile or end-state, depends on the magnitude of the viscosity. Some properties of the shock equation are demonstrated by deriving analytical expressions for shock structure in the weak-shock limit. The weak shock assumption provides further clarity concerning the balance between steepening and viscous diffusion and the role of the viscous formulation in determining the Bernoulli drop in each layer. Newtonian and non-Newtonian viscous formulations give slightly different end-states and Bernoulli drops.

Numerical solutions of the finite amplitude shock equations provide further insight. First, the prescription of boundary conditions using viscous tail modes proves shock uniqueness and clarifies the meaning of the steepening condition. Second, the numerical solutions verify the weak-shock formulae and determine their range of validity. Third, a shock bifurcation is found. Beyond a certain Froude number, steady state shocks suddenly cease to exist even though a range of subcritical states is available. This occurs when the shock is so strong that the end state recrosses the critical curve, i.e., the physical end state does not lie in the subcritical regime. With the end state back in the supercritical regime, steepening is absent.

In the last section, we used a 2-D, time-dependent, flux-form shallow water model (SWM) to investigate how shocks might form in real flows. The numerical results show that a strong bow-shock, upstream of an obstacle, suddenly disappears when the ambient condition reaches the condition for shock bifurcation. The SWM also gives a reasonable prediction of Bernoulli loss in each layer, indicating that it may be used for the investigation of potential vorticity generation.

Finally, to put our theory in perspective, we offer a brief comparison between ideal shock theory and Yih-Guha theory. These theories share the assumption of no mixing of mass or momentum between layers. YG has been compared with experimental data in several previous studies (YG55 and Baines, 95). Our comparing with YG can be considered an indirect way to compare with experimental data.

Ideal shock theory formulates a viscous model equation. One solubility condition for this equation is related to the steepening hypothesis. Satisfaction of the energy-loss principle is guaranteed in both layers by the viscous formulation; it is not used to select roots. The ideal shock theory can be used to predict the Bernoulli drop in each layer.

Y-G theory uses an approximate closure condition for momentum exchange to identify those states for which mass and momentum conserving conjugate states exist. It equates the existence of conjugate states, with net Bernoulli drop, with shock existence. While it makes some remarkably useful predictions, it also contains inconsistencies. (a) It has spurious secondary roots (i.e., unphysical end states). These roots can be removed by employing a steepening or layer-wise energy-loss principle. (b) Even its primary root can have a supercritical end state. These cases can be removed by employing the steepening criterion. (c) The primary root has a Bernoulli rise in the contracting layer. This problem can only be corrected with an ad hoc alteration in the YG closure condition. Thus, YG theory cannot be used to predict the partitioning of Bernoulli loss between layers.

While the Y-G inconsistencies are troubling, they are quantitatively small in most cases. Thus, comparison of ideal shock theory or Y-G theory with existing experimental data would yield similar agreement. Neither theory would capture the proper speed of strong internal bores (with mixing) discussed by KRS97.

The ideal shock theory is more complex than Y-G theory, but it avoids the Y-G inconsistencies and does not require an ad hoc choice of a momentum exchange formula or Bernoulli drop. It is difficult to clearly define the valid range of our theory. If the contribution from mixing and non-hydrostatic terms were proportional to the shock strength (i.e., $\propto (h_b - h_a)/h_a$), our theory requires $(h_b - h_a)/h_a \ll 1$. Comparing with experimental data suggests that for both bores and jumps, our theory agrees with experimental data well until $(h_b - h_a)/h_a > 0.4$.

8. Acknowledgments

Christoph Schär kindly allowed us to use his shallow water code. Paul Gluhosky assisted with software support. This research was supported by the National Science Foundation, Division of Atmospheric Sciences (ATM-9711076).

9. Appendix A

Computing Bernoulli loss

For a two-layer flow with a rigid lid, in a viscous shock (jump/drop), we have:

$$M_1 = \frac{Q_1^2}{H} + \frac{1}{2} gH^2 + rgH(D-H) + PH, \tag{A.1}$$

$$M_2 = \frac{Q_2^2}{D-H} + \frac{1}{2} g(D-H)^2 + P(D-H), \tag{A.2}$$

$$B_1 = \frac{Q_1^2}{2H^2} + gH + rg(D-H) + P, \tag{A.3}$$

$$B_2 = \frac{Q_2^2}{2(D-H)^2} + gD + P, \tag{A.4}$$

where $M_1 = M_1(x)$ and $M_2 = M_2(x)$ are generalized momentum in the lower/upper layer, $B_1 = B_1(x)$ and $B_2 = B_2(x)$ are Bernoulli functions in the lower/upper layer, $P = P(x)$ is the pressure at the rigid lid, and $H = H(x)$ is the lower layer depth.

Taking derivatives of (A.1), (A.2), (A.3), and

(A.4) with respect to x, we obtain

$$\frac{dM_1}{dx} = \left(-\frac{Q_1^2}{H^2} + gH + rgD - 2rgH + P\right)H_x + HP_x, \tag{A.5}$$

$$\frac{dM_2}{dx} = \left(\frac{Q_2^2}{(D-H)^2} - g(D-H) - P\right)H_x + (D-H)P_x, \tag{A.6}$$

$$\frac{dB_1}{dx} = \left(-\frac{Q_1^2}{H^3} + g'\right)H_x + P_x, \tag{A.7}$$

$$\frac{dB_2}{dx} = \frac{Q_2^2 H_x}{(D-H)^3} + P_x. \tag{A.8}$$

Therefore,

$$\frac{dB_1}{dx} = \frac{1}{H}\frac{dM_1}{dx} - \frac{PH_x}{H} - \frac{rg(D-H)H_x}{H}, \tag{A.9}$$

$$\frac{dB_2}{dx} = \frac{1}{D-H}\frac{dM_2}{dx} + \frac{PH_x}{D-H} + gH_x. \tag{A.10}$$

Using (13, 14) we have

$$\frac{dB_1}{dx} = \frac{f_{1x}}{H}, \tag{A.11}$$

$$\frac{dB_2}{dx} = \frac{f_{2x}}{D-H}. \tag{A.12}$$

Using (15, 16) we obtain

$$\frac{dB_1}{dx} = -\frac{Q_1}{H}\left(\frac{v_{1x}H_x}{H} + \frac{v_1 H_{xx}}{H} - \frac{v_1}{H^2}(H_x)^2\right), \tag{A.13}$$

$$\frac{dB_2}{dx} = \frac{Q_2}{D-H}\left(\frac{v_{2x}H_x}{D-H} + \frac{v_2 H_{xx}}{D-H)} - \frac{v_2}{(D-H)^2}(H_x)^2\right). \tag{A.14}$$

Expand (A.13) and (A.14) about the critical depth (H_c) in a Taylor series, and drop the high order terms. For the lower layer, we have:

$$\frac{dB_1}{dx} = -\frac{Q_1}{H_c^2}(v_{1x}\eta_x + v_1\eta_{xx})\left(1 - 2\frac{\eta}{H_c}\right) + \frac{Q_1}{H_c^3}v_1(\eta_x)^2 + O(\eta^3). \tag{A.15}$$

Eq. (A.15) can be rewritten as

$$\frac{dB_1}{dx} = -\frac{Q_1}{H_c^2}(v_{1x}\eta_x)_x + \frac{2Q_1}{H_c^3}(v_1\eta\eta_x)_x - \frac{Q_1}{H_c^3}v_1(\eta_x)^2 + O(\eta^3). \tag{A.16}$$

The first two terms on the r.h.s. eq. (A.16) are exact derivatives. Integrating from point a to point b, we get:

$$\Delta B_1 = B_{1b} - B_{1a} = \frac{Q_1}{H_c^3}\int_a^b v_1(\eta_x)^2\,dx + \text{h.o.t.}. \tag{A.17}$$

Similarly for the upper layer, to second order, we obtain

$$\frac{dB_2}{dx} = \frac{Q_2(v_{2x}\eta_x)_x}{(D-H_c)^2} - 2\frac{Q_2}{(D-H_c)^3}(v_2\eta\eta_x)_x + \frac{v_2 Q_2(\eta_x)^2}{(D-H_c)^3} + O(\eta^3). \tag{A.18}$$

Again, the first two terms in (A.18) are exact derivatives. Integrating (A.18) from a to b, we obtain

$$\Delta B_2 = B_{2b} - B_{2a} = \frac{Q_2}{(D-H_c)^3}\int_a^b v_2(\eta_x)^2\,dx + \text{h.o.t.}. \tag{A.19}$$

Eqs. (A.17) and (A.19) are given in the text as (35) and (36).

10. Appendix B

Rescaling of the SWM solutions with a upper free surface

For a 2-layer flow with an upper free surface, there are two wave modes, the internal gravity wave and the external gravity wave. As the density ratio r approach unity, while the external speed (relative to the mean flow) slightly increases, the internal wave speed goes to zero. As is well known, if the flow speed is close to the internal wave speed, the internal mode, which is related to the lower interface, is much more active, and the upper free surface is almost unchanged. This knowledge allows us to use a two-layer free-surface model to model the internal dynamics of a two layer Boussinesq flow under a rigid lid.

The critical condition for two layer flow to have zero wave speed is:

$$(F_1^2 - 1)(F_2^2 - 1) = r. \tag{B.1}$$

For the first part of the study, we are only interested in flow with small Froude numbers (i.e., $F_1, F_2 \ll 1$). For this range of Froude number, as will be shown, the upper free surface is nearly flat, similar to the rigid lid shock solutions. In this limit, the higher order term $(F_1^2 F_2^2)$ in eq. (B.1) can be ignored. The eq. (.20) can be rewritten as

$$F_1'^2 + F_2'^2 = 1, \tag{B.2}$$

where $F'_{1,2} = F_{1,2}/\sqrt{1-r}$. Eq. (.21) is identical with eq. (4) for the rigid lid case.

REFERENCES

Armi, L. 1986. The hydraulics of two flowing layers of different densities. *J. Fluid Mech.* **163**, 27–58.

Baines, P. G. 1984. A unified description of two-layer flow over topography. *J. Fluid Mech.* **146**, 127–167.

Baines, P. G. 1995. *Topographic effects in stratified flows.* Cambridge University Press, 488 pp.

Baines, P. G. and Davies, P. A. 1980. Laboratory studies of topographic effects in rotating and/or stratified fluids. GARP Pub. Ser. 23, Orographic Effects in Planetary Flows, ICSU/WMO, pp. 233–299.

Benjamin, T. B. 1968. Gravity currents and related phenomena. *J. Fluid Mech.* **31**, 209–248.

Chu, V. H. and Baddour, R. E. 1977. Surges, waves and mixing in two layer density stratified flow. Proc. 17th Congr. *Intl Assn Hydraul. Res.* **1**, 303–310.

Davies, H. C. 1983. Limitations of some common lateral boundary schemes in regional NWP models. *Mon. Wea. Rev.* **111**, 1002–1012.

Grubišić, V., Smith, R. B. and Schär, C. 1995. The effect of bottom friction on shallow-water flow past an isolated obstacle. *J. Atmos. Sci.* **52**, 1985-2005.

Gustafsson, B. and Sundstrom, A. 1978. Incompletely parabolic problems in fluid dynamics. *SIAM J. Appl. Math.* **35**, 343–357.

Hayakawa. N. 1970. Internal hydraulic jump in coherent stratified flow. *J. of the Engineering Mechanics Division* (ASCE) **96**, no. EM5, 797–800.

Houghton, D. D. C. 1964. An example of interaction between finite-amplitude gravity waves. *J. Atmos. Sci.* **21**, 493–499.

Houghton, D. D. C. and Kasahara, A. 1968. Nonlinear shallow fluid flow over an isolated ridge. *Commun. Pure Appl. Maths.* **21**, 1–23.

Houghton, D. D. C. and Isaacson, E. 1968. Mountain winds. *Studies in Num. Anal.* **2**, 21–52.

Jiang, Q. and Smith, R. B. 2000. V-wave, bow wave, and wakes in supercritical hydrostatic flow. *J. Fluid Mech.* **406**, 27–53.

Jiang, Q. and Smith, R. B. 2001. Ideal shocks in two layer flow, Part II: Under a passive layer. *Tellus* **53A**, 146–167.

Klemp, J. B., Rotunno, R. and Skamarock, W. C. 1997. On the propagation on internal bores. *J. Fluid Mech.* **331**, 81–106.

Long, R. R. 1954. Some aspects of the flow of stratified fluids (II). Experiments with a two-fluid system. *Tellus* **6**, 97–115.

Long, R. R. 1970. Blocking effects in flow over obstacles. *Tellus* **22**, 471–480.

Long, R. R. 1972. Finite amplitude disturbances in the flow of inviscid rotating and stratified fluids over obstacles. *Ann. Rev. Fluid Mech.* **4**, 69–92.

Mehrotra, S. C. 1973. Limitation on the existence of shock solutions in a two fluid system. *Tellus* **15**, 169–173.

Mehrotra, S. C. and Kelly, R. E. 1973. On the question of non-uniqueness of internal hydraulic jumps and drops on a two fluid system. *Tellus* **15**, 560–567.

Pan, F. and Smith, R. B. 1999. Gap winds and wakes: SAR observations and numerical simulations. *J. Atmos. Sci.* **56**, 905–923.

Rottman, J. W. and Simpson, J. E. 1989. The formation of internal bores in the atmosphere: a laboratory model. *Quart. J. Roy. Meteo. Soc.* **115**, 941–963.

Rouse, H., Siao, T. T. and Nagaratnam, S. 1959. Turbulence characteristics of the hydraulic jumps. *Trans. Amer. Soc. Civ. Eng.* **124**, 926–966.

Schär, C. and Smith, R. B. 1993. Shallow-water flow past an isolated topography. Part I: Vorticity production and wake formation. *J. Atmos. Sci.* **50**, 1373–1400.

Schär, C. and Smolarkiewicz, P. K. 1996. A synchronous and iterative flux-correction formalism for coupled transport equations. *J. Comput. Phys.* **128**, 101–120.

Smith, R. B. 1977. Formation of folds, boudinage, and mullions in non-Newtonian materials. *Geological Society of America Bulletin* **88**, 312–320.

Smith, R. B. and Smith, D. F. 1995. Pseudoviscid wake formation by mountains in shallow water flow with a drifting vortex. *J. Atmos. Sci.* **52**, 436–454.

Smith R. B., Gleason, A. C., Gluhosky, P. A. and Grubišić, V. 1997. The wake of St. Vincent. *J. Atmos. Sci.* **54**, 606–623.

Whitham, G. B. 1974. *Linear and non-linear waves.* Wiley and Sons, New York, 636 pp.

Wood, I. R. and Simpson, J. E. 1984. Jumps in layered miscible fluids. *J. Fluid Mech.* **140**, 329–342.

Yih, C. S. and Guha, C. R. 1955. Hydraulic jump in a fluid system of two layers. *Tellus* **7**, 358–366.